

Diffraction effects in few-cycle optical pulses

Miguel A. Porrás

Departamento de Física Aplicada, Escuela Técnica Superior de Ingenieros de Minas, Universidad Politécnica de Madrid, Ríos Rosas 21, E-28003 Madrid, Spain

(Received 16 September 2001; published 22 January 2002)

Basic concepts of three-dimensional wave packets are applied to the description of transverse effects on the propagation of ultrashort (femtosecond) pulses. The frequency-dependent nature of diffraction acts as a kind of dispersion that modifies the pulse front surface, its group velocity, the envelope form, and the carrier frequency. If the diffracted field in the monochromatic case is known, these changes can be straightforwardly quantified. Finding the propagated pulsed beam field reduces to a well-known and simpler problem of one-dimensional pulse propagation with group velocity dispersion. The method is applied to pulsed Gaussian beams and pulsed Bessel beams. Anomalous pulse front behavior, including superluminality in pulsed Gaussian beams is found. The carrier phase at any point of space is calculated.

DOI: 10.1103/PhysRevE.65.026606

PACS number(s): 42.25.Bs, 42.25.Fx, 42.65.Tg, 42.60.Jf

I. INTRODUCTION

Diffraction of ultrashort, femtosecond light pulses, and, in particular, the effects of diffraction in their temporal form has received considerable attention in the last few years [1–7]. Femtosecond pulses comprising only a few optical oscillations can now be almost routinely generated [8]. Changes in their temporal form during propagation in free space or material media due to their finite transversal size should be taken into account. In fact, these have been shown to play an essential role in the design of experiments with femtosecond pulses [8], particularly in their nonlinear interactions with matter [9].

Diffraction-induced pulse transformations of femtosecond pulses with a Gaussian transversal profile have been studied in a number of papers [1–3]. They revealed interesting effects such as pulse front curvature (time delay), pulse broadening, spectral changes leading to redshift or blueshift of optical oscillations, and the time-derivative effect at the far field. Due to the lack of closed-form analytical expressions for the propagated field, most of these phenomena have been described qualitatively from numerical simulations [1], from particular on-axis [3] or asymptotic expressions at the field [1], or from inspection of the corresponding spectra [2].

As claimed in Ref. [3], there is need of a simple theory of diffraction of femtosecond pulses, comparable in its simplicity to that of monochromatic Gaussian beams. The present paper represents an effort in that direction. By using elemental concepts on the propagation of three-dimensional wave packets [10] such as the pulse front surface, its group velocity, and group velocity dispersion, we can describe and classify the above effects (and others) in a natural order, write down simple accurate analytical expressions for them and for the propagated field of general (non-Gaussian) pulsed beam sources at any point of space. Diffraction-induced transformation of pulses is expressed in the familiar language of one-dimensional pulse propagation in media with phase and gain dispersion [11].

We apply this method to obtain a detailed characterization of the field of pulsed Gaussian beams and pulsed Bessel beams. In the first case, we find some unnoticed features

such as pulse front and wave front with opposite curvatures within the Rayleigh range and superluminality outside this range. Particular attention is paid to changes in the “carrier phase,” or in the relative position of the carrier oscillations with respect to the envelope, an essential parameter in the phase-sensitive nonlinear interactions of femtosecond pulses [8,9]. An accurate expression for the carrier phase at any point of space is provided.

Throughout this paper, a function of time $f(t)$ will be represented by its complex analytic signal $F(t)$ [12], whose real part gives $f(t)$. The real and imaginary parts of $F(t)$ are Hilbert transform pairs [10]. If the frequency spectrum of $f(t)$ is \hat{f}_ω , i.e.,

$$f(t) = \frac{1}{2\pi} \int_{-\infty}^{\infty} d\omega \hat{f}_\omega \exp(-i\omega t), \quad (1)$$

then the frequency spectrum of the analytic signal is $\hat{F}_\omega = 2\theta(\omega)\hat{f}_\omega$, where $\theta(\cdot)$ is the Heaviside step function. The analytic signal

$$F(t) = \frac{1}{\pi} \int_0^{\infty} d\omega \hat{f}_\omega \exp(-i\omega t) \quad (2)$$

thus has no negative frequencies and the positive ones are doubled. In this paper, the symbols Δt and $\Delta\omega$ will mean full width at half maximum (FWHM) of $|F(t)|^2$ and $|\hat{f}_\omega|^2$, respectively.

II. THEORY

A. Preliminaries

We consider a spatially and temporally localized optical disturbance $E(\mathbf{r}_\perp, t)$, $\mathbf{r}_\perp \equiv (x, y)$ of the frequency spectrum $\hat{E}_\omega(\mathbf{r}_\perp)$ at a certain plane $z=0$ of a suitable Cartesian coordinate system, and study how the radiated field $E(\mathbf{r}, t)$, $\mathbf{r} \equiv (x, y, z)$ propagates in the half space $z>0$.

Without loss of generality, we shall conveniently write the frequency spectrum of the initial disturbance in the form

$\hat{E}_\omega(\mathbf{r}_\perp) = \hat{p}_\omega \hat{U}_\omega(\mathbf{r}_\perp)$ with $\hat{U}_\omega(\mathbf{r}_\perp=0) = 1$. In this way \hat{p}_ω is the frequency spectrum at the point $\mathbf{r}_\perp=0$, a representative point of the source about which the source is approximately located, and

$$P(t) = \frac{1}{\pi} \int_0^\infty \hat{p}_\omega \exp(-i\omega t) d\omega \quad (3)$$

is the temporal wave form at this point. The function $U_\omega(\mathbf{r}_\perp)$ represents a monochromatic disturbance of frequency ω and normalized amplitude. If the spectrum $\hat{E}(\mathbf{r}_\perp, t) = \hat{p}_\omega \hat{U}_\omega(\mathbf{r}_\perp)$ factorizes into a function of frequency and a function of position, i.e., if $\hat{U}_\omega(\mathbf{r}_\perp) = U(\mathbf{r}_\perp)$ does not depend on frequency, the source is said to be spectrally pure. In this case, monochromatic disturbances of different frequencies have the same transversal profile $U(\mathbf{r}_\perp)$ [apart from their variable amplitude \hat{p}_ω], and all points of the source present the temporal field variation $P(t)$ (apart from a global amplitude $U(\mathbf{r}_\perp)$).

Beyond the source ($z > 0$), the frequency spectrum $\hat{p}_\omega \hat{U}_\omega(\mathbf{r})$ of the radiated field $E(\mathbf{r}, t)$ is determined by the Helmholtz equation $\Delta \hat{U}_\omega(\mathbf{r}) + (\omega/c)^2 \hat{U}_\omega(\mathbf{r}) = 0$, or by the paraxial wave equation for the slowly varying complex amplitude $\psi_\omega(\mathbf{r})$ [$\hat{U}_\omega(\mathbf{r}) = \psi_\omega(\mathbf{r}) \exp(i\omega z/c)$];

$$\Delta_\perp \psi_\omega(\mathbf{r}) + 2i \frac{\omega}{c} \frac{\partial \psi_\omega(\mathbf{r})}{\partial z} = 0, \quad (4)$$

if the monochromatic light beam $\hat{U}_\omega(\mathbf{r})$ is highly directional along the z direction. In the preceding equations Δ and Δ_\perp are the Laplacian and transversal Laplacian operators, respectively, and c is the speed of light in vacuum.

Propagation transforms $\hat{U}_\omega(\mathbf{r})$ into a function of frequency if it was not at the source. The same can be said for its real amplitude $a_\omega(\mathbf{r}) > 0$ and phase $\varphi_\omega(\mathbf{r})$ ($\hat{U}_\omega(\mathbf{r}) = a_\omega(\mathbf{r}) \exp[i\varphi_\omega(\mathbf{r})]$). In the trivial case of a plane wave [$\hat{U}_\omega(\mathbf{r}_\perp) = 1$], the dependence on frequency is the linear phase $\hat{U}_\omega(\mathbf{r}) = \exp(i\omega z/c)$, or $a_\omega(\mathbf{r}) = 1$ and $\varphi_\omega(\mathbf{r}) = \omega z/c$, but for a transversally localized disturbance $\hat{U}_\omega(\mathbf{r}_\perp)$ a more complicated dependence arises as a result of the frequency-dependent nature of diffraction. For instance, the paraxial wave equation (4) imposes the propagated field from the source $\hat{U}_\omega(\mathbf{r}_\perp) = \psi_\omega(\mathbf{r}_\perp, z=0)$ to be of the form

$$\hat{U}_\omega(\mathbf{r}) = \psi_\omega\left(\mathbf{r}_\perp, c \frac{z}{\omega}\right) \exp\left(i \frac{\omega}{c} z\right), \quad (5)$$

where ω appears again in the linear phase and in the combination of variables $c z/\omega$. The latter dependence reflects the fact that diffraction changes are smaller as the frequency of the source increases, and does not exist at all in the geometrical limit $\omega \rightarrow \infty$. The amplitude $a_\omega(\mathbf{r}) = |\psi_\omega(\mathbf{r}_\perp, c z/\omega)|$ carries this diffraction-induced dependence on frequency, and the phase $\varphi_\omega(\mathbf{r}) = \omega z/c + \arg \psi_\omega(\mathbf{r}_\perp, c z/\omega)$ becomes a non-linear function of frequency. For nonparaxial light beams, the dependence of $\hat{U}_\omega(\mathbf{r})$, its amplitude, and phase on frequency cannot be factorized as in the simple way of Eq. (5).

The time-domain radiated field can be written in terms of the propagated spectrum $\hat{p}_\omega \hat{U}_\omega(\mathbf{r})$ as

$$E(\mathbf{r}, t) = \frac{1}{\pi} \int_0^\infty d\omega \hat{p}_\omega \hat{U}_\omega(\mathbf{r}) \exp(-i\omega t) d\omega, \quad (6)$$

or equivalently,

$$E(\mathbf{r}, t) = \frac{1}{\pi} \int_0^\infty d\omega \hat{p}_\omega a_\omega(\mathbf{r}) \exp\{-i[\omega t - \varphi_\omega(\mathbf{r})]\}. \quad (7)$$

The pulsed beam $E(\mathbf{r}, t)$ can be said to be paraxial if all composing monochromatic light beams $\hat{U}_\omega(\mathbf{r})$ having significant amplitude \hat{p}_ω are paraxial. A more specific expression for paraxial pulsed beams can then be written by introducing $a_\omega(\mathbf{r}) = |\psi_\omega(\mathbf{r})|$, $\varphi_\omega(\mathbf{r}) = \omega z/c + \arg \psi_\omega(\mathbf{r})$ into Eq. (7).

Equation (7) describes the diffraction of a pulse in free space in the same way as a problem of pulse propagation in a medium with phase and gain dispersion, and as such could be treated with the numerical and asymptotic methods developed for that purpose [13].

B. Few-cycle pulsed beams

Our main concern in this paper is the propagation of pulsed beams whose temporal form consists of a few oscillations of a certain mean optical frequency, as those produced by the femtosecond laser devices developed in the 1990s [8]. In this case, the analysis of Eq. (7) can be greatly simplified by using a similar method to that of the heuristic theory of dispersive pulse propagation [13,14].

First, it has been shown that the description of pulses in terms of an envelope and carrier oscillations remains useful and physically meaningful for few-cycle pulses, even in the extreme case of pulses with only one oscillation [15]. Second, diffraction changes in the temporal form of few-cycle pulses have been shown to be generally small [5,6] (contrary to the case of subcycle pulses [3,16]). For these reasons, it seems appropriate to write the temporal form of the pulsed beam as enveloped carrier oscillations of the same carrier frequency ω_0 at any point of space,

$$E(\mathbf{r}, t) = A(\mathbf{r}, t) \exp\{-i[\omega_0 t - \varphi_{\omega_0}(\mathbf{r}) - \phi]\}, \quad (8)$$

where $A(\mathbf{r}, t)$ is a complex envelope and ϕ is an arbitrary phase (to be specified). In particular, since $E(0, t) = P(t)$ and $\varphi_{\omega_0}(0) = 0$,

$$P(t) = A(0, t) \exp[-i(\omega_0 t - \phi)]. \quad (9)$$

The exact choice of carrier frequency is not crucial [10,8]; for convenience, ω_0 will be defined as the ‘‘gravity center’’ of the pulsed beam spectral intensity, and its exact value will be fixed at $\mathbf{r}=0$, i.e.,

$$\omega_0 = \frac{\int_0^\infty d\omega \omega |\hat{p}_\omega|^2}{\int_0^\infty d\omega |\hat{p}_\omega|^2}. \quad (10)$$

The phase ϕ is usually chosen so that $A(0,t)$ is real at the origin of time $t=0$, a time that is usually made to coincide with an important feature of $P(t)$, for instance, the maximum of the absolute amplitude $|A(0,t)|$ (if there is only one; otherwise, one can choose its ‘‘gravity center’’). Defined in this way, the phase ϕ is referred to as the carrier phase and determines the ‘‘position’’ of the carrier oscillations with respect to the envelope. This parameter has been shown to play an important role in nonlinear interactions of few-cycle pulses.

The complex envelope $A(\mathbf{r},t)$ modulates (spatially and temporally) the phase and the amplitude of the oscillations of the monochromatic light beam of the carrier frequency, and is given from Eqs. (7) and (8) by

$$A(\mathbf{r},t) = \frac{1}{\pi} \int_0^\infty d\omega \hat{p}_\omega a_\omega(\mathbf{r}) \exp\{-i[(\omega - \omega_0)t - \varphi_\omega(\mathbf{r}) + \varphi_{\omega_0}(\mathbf{r}) + \phi]\}. \quad (11)$$

In particular, at $\mathbf{r}=0$,

$$A(0,t) = \frac{1}{\pi} \int_0^\infty \hat{p}_\omega \exp\{-i[(\omega - \omega_0)t + \phi]\}. \quad (12)$$

Comparison of Eqs. (11) and (12) shows that changes in the temporal form of the envelope during propagation originate from the dependence of $a_\omega(\mathbf{r})$ on frequency and the nonlinear dependence of $\varphi_\omega(\mathbf{r})$ on frequency (a linear dependence simply translates the envelope) due to diffraction. We also observe that the integration domain in Eq. (11) is effectively limited to the small interval $\Delta\omega$ about ω_0 ($\Delta\omega/\omega_0 \ll 1$) where \hat{p}_ω takes significant values (a N -cycle pulse with Gaussian envelope, for instance, satisfies $\Delta\omega/\omega_0 \approx 0.44/N$). It is then expedient to express the variation with frequency of $\varphi_\omega(\mathbf{r})$ within the interval $\Delta\omega$ as a Taylor series about ω_0 ,

$$\varphi_\omega(\mathbf{r}) = \varphi_{\omega_0}(\mathbf{r}) + \varphi'_{\omega_0}(\mathbf{r})(\omega - \omega_0) + \frac{1}{2} \varphi''_{\omega_0}(\mathbf{r})(\omega - \omega_0)^2 + \dots, \quad (13)$$

where the prime sign means differentiation with respect to ω . Equation (11) for the envelope then becomes

$$A(\mathbf{r},t) = \frac{1}{\pi} \int_0^\infty d\omega \hat{p}_\omega a_\omega(\mathbf{r}) \exp\left\{\frac{i}{2}(\omega - \omega_0)^2 \varphi''_{\omega_0}(\mathbf{r}) + \dots\right\} \times \exp\{-i[(\omega - \omega_0)(t - \varphi'_{\omega_0}(\mathbf{r})) + \phi]\}, \quad (14)$$

where $a_\omega(\mathbf{r})$ can also be expanded in a Taylor series as

$$a_\omega(\mathbf{r}) \approx a_{\omega_0}(\mathbf{r}) + a'_{\omega_0}(\mathbf{r})(\omega - \omega_0) + \dots. \quad (15)$$

It turns out that all predicted phenomena in the diffraction of few-cycle pulsed Gaussian beams find explanation from the consideration of the different terms explicitly written in Eqs. (14) and (15), phenomena that appear now to occur, in one form or another, during propagation of more general pulsed beams. In fact, the form of Eqs. (8) and (14), together with Eq. (15), allows us to draw the following approximate picture of a propagating pulsed beam.

1. Up to the zero order in the amplitude and first order in the phase

The phase fronts or surfaces of equal phase, $\omega_0 t - \varphi_{\omega_0}(\mathbf{r}) = \text{const}$, of the pulsed beam propagate at the phase velocity [10]

$$v^{(p)}(\mathbf{r}) = \frac{\omega_0}{|\text{grad } \varphi_{\omega_0}(\mathbf{r})|}. \quad (16)$$

The instant of time at which the pulse peaks [$|A(\mathbf{r},t)|$ is maximum] at position \mathbf{r} is given by [10]

$$t = \varphi'_{\omega_0}(\mathbf{r}). \quad (17)$$

This equation defines pulse front surface, which advances at the group velocity [10]

$$v^{(g)}(\mathbf{r}) = \frac{1}{|\text{grad } \varphi'_{\omega_0}(\mathbf{r})|}. \quad (18)$$

The quantity $\varphi'_{\omega_0}(\mathbf{r})$ thus measures the time of arrival of the pulse at position \mathbf{r} . The time delay induced by diffraction, or delay with respect to a plane pulse, is given by $\varphi'_{\omega_0}(\mathbf{r}) - z/c$.

From the knowledge of the phase and pulse fronts, it is possible to determine the carrier phase $\phi(\mathbf{r})$ at any position of space \mathbf{r} . From Eq. (8), the phase of the oscillations at the time $t = \varphi'_{\omega_0}(\mathbf{r})$ of the pulse peak is

$$\phi(\mathbf{r}) = \phi + \varphi_{\omega_0}(\mathbf{r}) - \omega_0 \varphi'_{\omega_0}(\mathbf{r}). \quad (19)$$

We note that, as in the approximate theory of one-dimensional dispersive pulse propagation, the equation $t = \varphi'_{\omega_0}(\mathbf{r})$ and Eq. (18) strictly define the pulse peak and its propagation velocity in the limit of small change of pulse form on propagation [10], as we are assuming. On the contrary, small deviations from the true location and velocity of the pulse may occur. In this case, pulse front and group velocity are commonly understood and used as measures of the approximate location and velocity of the pulse as a whole.

2. Up to first order in the amplitude and second order in the phase

Since $a_\omega(\mathbf{r})$ depends on frequency, the spectral amplitude $a_\omega(\mathbf{r})$ will change from point to point in space. These spectral changes have been studied for pulsed Gaussian beams in Ref. [2], in which case they lead to a small redshift of the carrier oscillations [1] along the transversal direction and a

blueshift along the axial direction [2]. For isodiffracting pulsed Gaussian beams, there is only redshift towards the beam periphery [5]. Physically, spectral changes in amplitude can be understood from a relative increase of the weight of redder (bluer) spectral components diffracted at larger (smaller) angles.

The amplitude spectrum $|\hat{p}_\omega|a_\omega(\mathbf{r})$ tends to shift towards bluer frequencies at points \mathbf{r} where $a'_{\omega_0}(\mathbf{r}) > 0$, and towards redder frequencies where $a'_{\omega_0}(\mathbf{r}) < 0$. The local frequency of the oscillations can be calculated from

$$\omega_0(\mathbf{r}) = \frac{\int_0^\infty d\omega \omega |\hat{p}_\omega|^2 a_\omega^2(\mathbf{r})}{\int_0^\infty d\omega |\hat{p}_\omega|^2 a_\omega^2(\mathbf{r})} \quad (20)$$

and approached from Eq. (15) by

$$\omega_0(\mathbf{r}) = \omega_0 + \frac{2a'_{\omega_0}(\mathbf{r})}{a_{\omega_0}(\mathbf{r})} (\Delta\omega_{\text{rms}})^2, \quad (21)$$

where $\Delta\omega_{\text{rms}}$ is the root mean square width of $|\hat{p}_\omega|^2$.

The term with $\varphi''_{\omega_0}(\mathbf{r})$ introduces a space-dependent chirp in the pulse spectrum, which may lead to pulse broadening. This chirp explains the (rather) small pulse broadening at large transversal distances in pulsed Gaussian beams [1] and isodiffracting Gaussian beams [5]. This effect is more pronounced in nonparaxial pulsed Bessel beams, in which case it can be used to compensate the chirp of opposite sign that a pulse acquires during propagation in a dispersive medium, and therefore to eliminate pulse broadening [17]. Free-space spectrum chirping originates from angular dispersion due to diffraction, as shown in Ref. [17]. Specific formulas for pulse broadening as a function of φ''_{ω_0} are deferred to the examples.

Additional pulse transformations coming from higher-order derivatives could be significant in specific cases, but will not be considered here.

In conclusion, we see that the knowledge of the expression of the monochromatic light beam $\hat{U}_\omega(\mathbf{r}) = a_\omega(\mathbf{r})\exp[i\varphi_\omega(\mathbf{r})]$, particularly its derivatives with respect to frequency at ω_0 , allows us to describe the transformations experienced by a pulse due to its finite transversal size. It is also possible to construct an explicit expression for the complex envelope at any point of space that carries the pulse transformations as described above. Introducing Eq. (15) into Eq. (14) and retaining up to the second derivative of the phase and the first derivative of the amplitude, we obtain

$$A(\mathbf{r}, t) \approx a_{\omega_0}(\mathbf{r}) A_{\text{GVD}}[\varphi''_{\omega_0}(\mathbf{r}), t - \varphi'_{\omega_0}(\mathbf{r})] + ia'_{\omega_0}(\mathbf{r}) \frac{\partial}{\partial \tau} A_{\text{GVD}}[\varphi''_{\omega_0}(\mathbf{r}), t - \varphi'_{\omega_0}(\mathbf{r})], \quad (22)$$

where $A_{\text{GVD}}(\xi, \tau)$ is the standard integral

$$A_{\text{GVD}}(\xi, \tau) \equiv \frac{1}{\pi} \int_0^\infty d\omega \hat{p}_\omega \exp\left[\frac{i}{2}(\omega - \omega_0)^2 \xi\right] \times \exp[-i(\omega - \omega_0)\tau] \quad (23)$$

describing one-dimensional propagation of a pulse of envelope $A(0, \tau)$ in a medium with group velocity dispersion (GVD), an integral that can be analytically performed in certain cases. More accurate expressions carrying higher-order pulse transformations can also be constructed by adding the corresponding terms.

The above analysis is a convenient formulation and development of the fundamental concepts in relation with three-dimensional wave packets explained in Ref. [10]. Previous papers on propagation of pulsed beams, however, have not made use of these basic ideas, but have gone along other lines. The purpose of the remainder of this paper is to show its usefulness, accuracy, and capability of predicting new phenomena.

III. APPLICATION EXAMPLES

A. Pulsed Gaussian beam

We first consider the pulsed beam emitted by the pulsed Gaussian source

$$E(\mathbf{r}_\perp, t) = P(t) \exp(-r^2/s^2), \quad (24)$$

where $r^2 = x^2 + y^2$ and $P(t)$ is a pulse of carrier frequency ω_0 , envelope $A(0, t)$ that peaks at $t = 0$, and carrier phase ϕ . The propagation of pulsed Gaussian beams has been extensively studied in the past. Christov [1] obtained an expression for the far field and studied numerically the near field, describing qualitatively spectrum redshift, pulse time broadening and delay increasing towards the beam periphery, while Sheppard and Gan [2] described a spectrum blueshift along the propagation direction. The on-axis field was studied by Kaplan [3] in the cases of subcycle and multicycle pulses. Approximate expressions in the form of truncated series valid at any point of space have been reported recently [7]. The present method allows us to describe all previously described effects in quantitative terms, to find some new important features of pulsed Gaussian beams, and to write a simple approximate expression for their propagating field.

The spectrum of Eq. (24) is $\hat{E}_\omega(\mathbf{r}_\perp) = \hat{p}_\omega \exp(-r^2/s^2)$; then $\hat{U}_\omega(\mathbf{r}_\perp) = \exp(-r^2/s^2)$ is independent of frequency. If all frequencies in the frequency band $\Delta\omega$ of the pulse $P(t)$ satisfy the paraxial condition $\lambda_\omega = 2\pi c/\omega \ll s$, then $\hat{U}_\omega(\mathbf{r})$ is given by the well-known Gaussian beam formula

$$\hat{U}_\omega(\mathbf{r}) = \frac{-iL_\omega}{q_\omega(z)} \exp\left[\frac{i\omega r^2}{2cq_\omega(z)}\right] \exp\left(i\frac{\omega}{c}z\right), \quad (25)$$

where $q_\omega(z) = z - iL_\omega$ is the so-called complex beam parameter, and $L_\omega = \omega s^2/2c$ is the diffraction length or Rayleigh distance for each frequency. The amplitude and phase of the monochromatic Gaussian beam in Eq. (25) are

$$a_\omega(\mathbf{r}) = \frac{s}{s_\omega(z)} \exp\left[-\frac{r^2}{s_\omega^2(z)}\right], \quad (26)$$

$$\varphi_\omega(\mathbf{r}) = \frac{\omega}{c}z - \tan^{-1}\left(\frac{z}{L_\omega}\right) + \frac{\omega r^2}{2cR_\omega(z)}, \quad (27)$$

where

$$s_\omega(z) = s \sqrt{1 + \frac{z^2}{L_\omega^2}}, \quad (28)$$

$$R_\omega(z) = z + \frac{L_\omega^2}{z}$$

are the Gaussian width and wave front radius of curvature, respectively, at any propagation distance.

The phase fronts of the pulsed Gaussian beam,

$$\omega_0 t - \frac{\omega_0}{c}z + \tan^{-1}\left(\frac{z}{L_{\omega_0}}\right) - \frac{\omega_0 r^2}{2cR_{\omega_0}(z)} = \text{const.}, \quad (29)$$

are spherical (in the paraxial approximation) of variable radius $R_{\text{phase}}(z) = R_{\omega_0}(z)$.

The derivative of the phase $\varphi_{\omega_0}(\mathbf{r})$ with respect to frequency, evaluated at the carrier frequency, is readily evaluated to be

$$\varphi'_{\omega_0}(\mathbf{r}) = \frac{z}{c} + \frac{z}{\omega_0 L_{\omega_0}} \frac{s^2}{s_{\omega_0}^2(z)} + \frac{r^2}{2cR_{\omega_0}^2(z)} \left(z - \frac{L_{\omega_0}^2}{z}\right). \quad (30)$$

The equation of the pulse front is then

$$t = \frac{z}{c} + \frac{z}{\omega_0 L_{\omega_0}} \frac{s^2}{s_{\omega_0}^2(z)} + \frac{r^2}{2cR_{\omega_0}^2(z)} \left(z - \frac{L_{\omega_0}^2}{z}\right), \quad (31)$$

which represents also a spherical surface (within the paraxial approximation) whose radius

$$R_{\text{pulse}}(z) = \frac{R_{\text{phase}}^2(z)}{z - \frac{L_{\omega_0}^2}{z}} \quad (32)$$

varies with propagation distance z , and is different from that of the wave fronts. The radii of the phase and pulse fronts versus propagation distance are shown in Fig. 1. The graphic shows the striking fact that the initial plane pulse front of pulsed Gaussian beams becomes convergent at first, reaching a minimum radius of absolute value $4L_{\omega_0}$ at $z = L_{\omega_0}/(1 + \sqrt{2}) = 0.4142L_{\omega_0}$. At the Rayleigh distance L_{ω_0} the pulse front is again plane, and at larger propagation distances becomes divergent, tending to match the phase fronts. The pulse front curvature is a consequence of the delay of arrival of the pulse [last term of Eq. (31)] at an off-axis point with respect to its arrival at the on-axis point on the same trans-

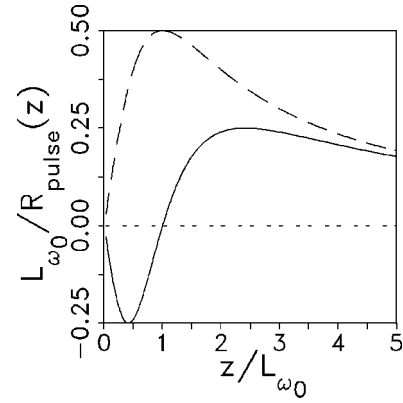


FIG. 1. Solid curve: curvature (inverse of the radius of curvature) of the pulse front of pulsed Gaussian beams as a function of the axial propagation distance. Dashed curve: curvature of the phase fronts.

versal plane z . Also, the time delay with respect to a plane pulse, or delay induced by diffraction, is given by the two last terms of Eq. (31). In Fig. 2 we confirm numerically the above results with a Gaussian pulse having $1 + 1/2$ oscillations. At $z < L_{\omega_0}$ [Fig. 2(a)], the envelope [numerically calculated from Eq. (11)] arrives earlier at an off-axis point (dashed curve) than at an on-axis point (solid curve), which means that the pulse front is converging. At $z > L_{\omega_0}$, the opposite is true, i.e., the pulse front appears to diverge.

The velocity of propagation of the phase fronts (29) was calculated in Ref. [18], and was found to be slightly subluminal ($< c$) at points $r > s_{\omega_0}(z)$ and superluminal at $r < s_{\omega_0}(z)$. The greater values of the phase velocity are reached at the beam axis ($r = 0$), their values being (see Fig. 3)

$$v^{(p)}(z) = \frac{c}{\left(1 - \frac{\theta_0^2}{1 + z^2/L_{\omega_0}^2}\right)}, \quad (33)$$

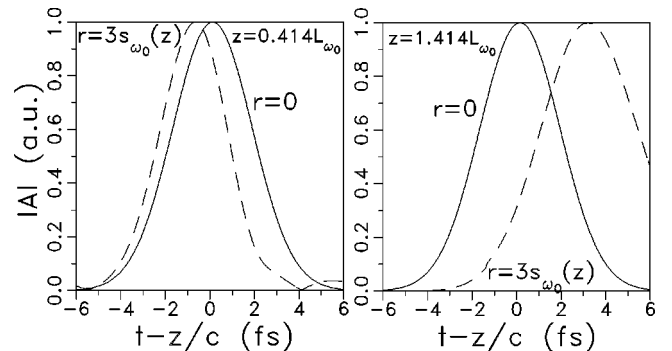


FIG. 2. Envelope temporal form at several positions after the source $E(\mathbf{r}_\perp, t) = \exp(-r^2/s^2)\exp(-t^2/b^2)\exp(-i\omega_0 t)$ with $\omega_0 = 3.2 \text{ fs}^{-1}$ (period $T_0 = 1.963 \text{ fs}$), $b = 2.50 \text{ fs}$ (FWHM of intensity $\Delta t = \sqrt{2 \ln 2} b = 1.5T_0$), and $s = 2 \text{ } \mu\text{m}$ ($L_{\omega_0} = 0.021 \text{ mm}$). At $z = 0.4142L_{\omega_0}$ the pulse arrives earlier at $r = 3s_{\omega_0}(z)$ than at $r = 0$. At $z = 1.4142L_{\omega_0}$ the pulse arrives earlier at $r = 0$ than at $r = 3s_{\omega_0}(z)$. Units of A are arbitrary.

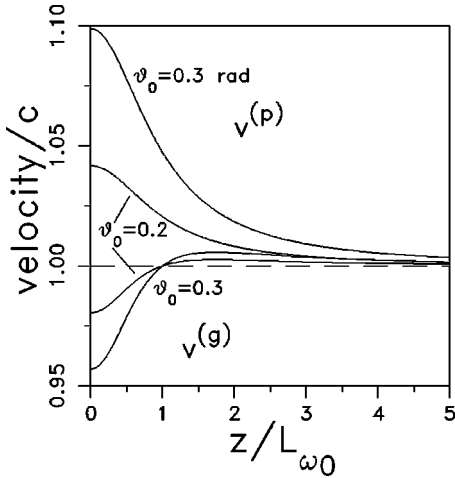


FIG. 3. On-axis phase and group velocities of pulsed Gaussian beams as functions of the propagation distance. Superluminality and subluminality of these quantities increases as the average divergence angle θ_0 (or divergence angle of the monochromatic Gaussian beam at the carrier frequency) is larger.

where $\theta_0 = 2c/\omega_0 s$ is the divergence angle of the monochromatic Gaussian beam at the carrier frequency. The velocity of propagation of the pulse front, calculated from Eq. (18), is given by

$$v^{(g)}(z) = \frac{c}{\left[1 + \frac{\theta_0^2}{2} \frac{1 - z^2/L_{\omega_0}^2}{(1 + z^2/L_{\omega_0}^2)^2} \right]}, \quad (34)$$

at on-axis points. The group velocity is subluminal at $z < L_{\omega_0}$ and superluminal at $z > L_{\omega_0}$, as shown in Fig. 3. Superluminality is more pronounced as the beam divergence is larger (i.e., as the source is narrower). Out of axis, $v^{(g)}$ is given by a much longer expression; its behavior is, however, similar except that subluminality at $z < L_{\omega_0}$ and superluminality at $z > L_{\omega_0}$ are less pronounced, as expected from the converging (diverging) form of the pulse front at $z < L_{\omega_0}$ ($z > L_{\omega_0}$). Group velocities faster than c have been reported recently in a number of waves propagating in free space, as in x waves [19], Bessel-x pulses [20], and Bessel-Gauss pulsed beams [21], but to our knowledge, not in Gaussian beams.

The carrier phase, or phase at pulse peak can be calculated from Eqs. (19), (29), and (31) to be

$$\phi(\mathbf{r}) = \phi - \tan^{-1}\left(\frac{z}{L_{\omega_0}}\right) - \frac{1}{\frac{z}{L_{\omega_0}} + \frac{L_{\omega_0}}{z}} \left[1 - \frac{2r^2}{s_{\omega_0}^2(z)} \right]. \quad (35)$$

The carrier-phase variation $\phi(\mathbf{r}) - \phi$ is plotted in Fig. 4 as a function of propagation distance z . The term $\tan^{-1}(z/L_{\omega_0})$ comes from Gouy's phase shift of the Gaussian beam at the carrier frequency (dashed curve), which ranges from 0 to $\pi/2$ at the far field, and is the only carrier-phase variation due to

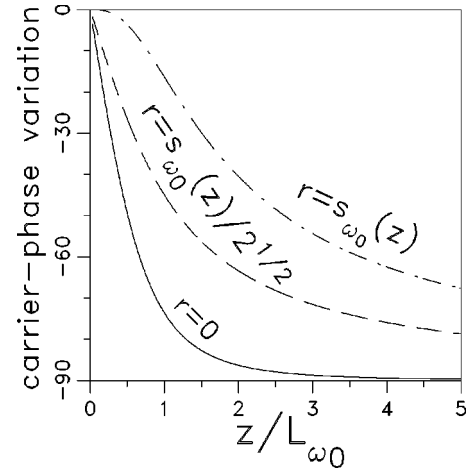


FIG. 4. Carrier phase variation $\phi(\mathbf{r}) - \phi$ with respect to the initial one, ϕ , for pulsed Gaussian beams as a function of axial propagation distance and for several radial positions.

diffraction previously described [8]. At on-axis points (solid curve) the carrier-phase variation is due to the Gouy phase shift plus the additional term $[(z/L_{\omega_0}) + (L_{\omega_0}/z)]^{-1}$, which can reach a value of about 30° at the Rayleigh distance. This additional phase originates from the advancement (on the beam axis) of the superluminal phase fronts with respect to the subluminal pulse front. Its net effect is to make the Gouy phase reach its asymptotic value faster. At off-axis points, since the phase fronts are always more curved than the pulse front, the situation may be reversed at large enough transversal distances (dash-dotted curve). The variation of the carrier phase due to curvature mismatch of the phase and pulse fronts is accounted for by the term with r^2 in Eq. (35). It is noticeable that on the revolution hyperboloid, or caustic surface $r = s_{\omega_0}/\sqrt{2}$, the two latter effects cancel (dashed curve), the carrier phase then being exactly given by the Gouy phase shift.

We point out that the pulse front equation (31), its curvature, velocity, and hence the carrier phase are the same irrespective of the pulse form and, in particular, of its duration. They can then be understood as properties of real Gaussian beams, which are never an infinitely long train of sinusoidal oscillations. The pulse front properties, however, are only relevant for few-cycle pulses, since the temporal (spatial) deviations of the pulse front with respect to the nondiffracted pulse front $t = z/c$ may be of the same order as the pulse duration (length), and hence involve drastic changes in the pulse amplitude.

On the contrary, diffraction-induced frequency shift in pulsed Gaussian beams does depend on pulse duration. From Eq. (26), the derivative with respect to frequency of $a_{\omega}(\mathbf{r})$, evaluated at the carrier frequency, can be calculated to be

$$a'_{\omega_0}(\mathbf{r}) = \frac{1}{\omega_0} \frac{1}{1 + \frac{L_{\omega_0}^2}{z^2}} \left[1 - \frac{2r^2}{s_{\omega_0}^2(z)} \right] a_{\omega_0}(\mathbf{r}). \quad (36)$$

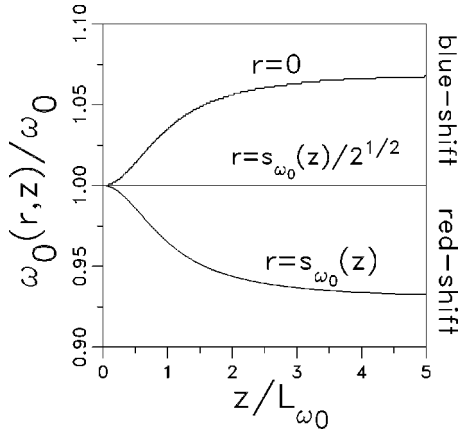


FIG. 5. Relative frequency shift of the optical oscillations in pulsed Gaussian beams as it varies with axial distance z along several caustic surfaces. On the caustic surface $r = s_{\omega_0}(z)/\sqrt{2}$ there is no frequency shift. The values are calculated for a single-cycle Gaussian pulse of Gaussian envelope, for which $\Delta\omega_{\text{rms}}/\omega_0 = 0.187$.

Again the revolution hyperboloid $r = s_{\omega_0}(z)/\sqrt{2}$, where $a'_{\omega_0}(\mathbf{r}) = 0$, plays an important role. There is no frequency shift on this surface, which separates the regions of blueshift ($a'_{\omega_0} > 0$ at $r < s_{\omega_0}(z)/\sqrt{2}$) and redshift [$a'_{\omega_0} < 0$ at $r > s_{\omega_0}(z)$]. The local frequency of the oscillations, calculated from Eqs. (21) and (36), is given by

$$\omega_0(\mathbf{r}) = \omega_0 \left\{ 1 + \frac{2}{1 + L_{\omega_0}^2/z^2} \left[1 - \frac{2r^2}{s_{\omega_0}^2(z)} \right] \left(\frac{\Delta\omega_{\text{rms}}}{\omega_0} \right)^2 \right\}, \quad (37)$$

and is represented in Fig. 5 as a function of the propagation distance for a single cycle pulse. In particular, along the beam axis, the blueshift is

$$\omega_0(z) = \omega_0 \left[1 + \frac{2}{1 + L_{\omega_0}^2/z^2} \left(\frac{\Delta\omega_{\text{rms}}}{\omega_0} \right)^2 \right], \quad (38)$$

which increases from zero up to the asymptotic value $\omega_0[1 + 2(\Delta\omega_{\text{rms}}/\omega_0)^2]$ in the far field, as shown in Fig. 5. As the number of oscillations in the pulse grows ($\Delta\omega_{\text{rms}} \rightarrow 0$), frequency shifts diminish and disappear in the many-cycle limit.

Diffraction-induced spectrum chirp, and hence pulse broadening, appear to be very small for pulsed Gaussian beams. We adopt here the convention that pulse broadening is negligible when the phase variation within the pulse frequency band due to its chirp is much smaller than 1 rad, i.e., when $(1/2)\varphi''_{\omega_0}(\mathbf{r})(2\Delta\omega_{\text{rms}})^2 \ll 1$. On account that $\Delta t_{\text{rms}}\Delta\omega_{\text{rms}} \sim 1/2$ for nearly dispersion limited pulses, the above inequality can be rewritten as

$$\varphi''_{\omega_0}(\mathbf{r}) \ll 2(\Delta t_{\text{rms}})^2. \quad (39)$$

This criterion is equivalent to the usual condition for negligible pulse broadening $z \ll L_{\text{disp}} = 2(\Delta t_{\text{rms}})^2/|k''_{\omega_0}|$ (dispersion length) when spectrum chirp originates from propagation in a material with group velocity dispersion k''_{ω_0} (second derivative of the propagation constant k_{ω_0}). Numerical inspection of the expression of $\varphi''_{\omega_0}(\mathbf{r})$ for Gaussian beams shows that condition (39) is satisfied for a single-cycle pulse upto transversal distances as large as $r = 5s_{\omega_0}(z)$. For pulses with more than one oscillation, this distance is even greater. Since at these distances peak intensity has fallen down below 10^{-21} times its value on the beam axis, we can write, to a good approximation, $\varphi''_{\omega_0}(\mathbf{r}) \approx 0$ where the intensity is significant.

In Fig. 6 we test numerically the previous results. This figure shows the propagated field of the initial Gaussian disturbance $E(\mathbf{r}_{\perp}) = P(t)\exp(-r^2/s^2)$, where $P(t) = \exp(-t^2/b^2)\exp(-i\omega_0 t)$ is a Gaussian pulse with zero carrier phase. We set $\omega_0 = 3.2 \text{ fs}^{-1}$ (period $T_0 = 1.96 \text{ fs}$), $b = 1.668 \text{ fs}$, and $s = 2 \mu\text{m}$ so that the pulse $P(t)$ contains only one oscillation within its FWHM duration ($\Delta t = \sqrt{2 \ln 2} b = T_0$), and the radiated pulsed beam can be regarded as paraxial. The temporal form of the propagated pulsed beam at several representative points of space (dots) was obtained by solving numerically integral (7) with $a_{\omega}(\mathbf{r})$ and $\varphi_{\omega}(\mathbf{r})$ given by Eqs. (26) and (27), respectively. For reference, we also show (dashed curves) the approximation obtained by neglecting all diffraction effects on pulse form (zero order in amplitude and phase), i.e., the pulsed beam $\exp[(t-z/c)^2/b^2]a_{\omega_0}(\mathbf{r})\exp[i\varphi_{\omega_0}(\mathbf{r})]\exp(-i\omega_0 t)$, whose envelope propagates without deformation along the plane pulse front $t = z/c$ at speed c . The meaning of the solid curves will be explained later.

We observe that at $z = 0.4142L_{\omega_0}$ (first column), $z = L_{\omega_0}$ (second column), and $z = 2.4142L_{\omega_0}$ (third column), the pulse front is slightly converging, nearly plane, and diverging, respectively, as expected from Eq. (32) for the pulse front radius. In fact, the corresponding delays of arrival at $r = s_{\omega_0}(z)\sqrt{2}$ with respect to the arrival at $r = 0$, estimated from the numerical data, are -0.18 , 0.00 , and 1.1 fs for the first, second, and third columns, respectively. The time delays from our analytical formula $r^2/2cR_{\text{pulse}}(z)$ [last term of Eq. (31)] are also -0.18 , 0.00 , and 1.1 fs .

The oscillations at on-axis points (bottom row) are always blueshifted with respect to ω_0 , the blueshift growing with propagation distance. Numerically calculated values of the frequencies are (a) 3.23, (d) 3.32, and (g) 3.39 fs^{-1} , in fair agreement with the values (a) 3.23, (d) 3.31, and (g) 3.39 fs^{-1} from Eq. (37). At the caustic surface $r = s_{\omega_0}(z)\sqrt{2}$ (upper row) the oscillations are instead redshifted. Numerically calculated frequencies are (c) 3.09, (f) 2.93, and (i) 2.71 fs^{-1} , to be compared with the approximate frequencies (c) 3.10, (f) 2.86, and (i) 2.63 fs^{-1} obtained from Eq. (37). At the caustic surface $r = s_{\omega_0}/\sqrt{2}$ (central row) frequency shift is negligible, as predicted by Eq. (37).

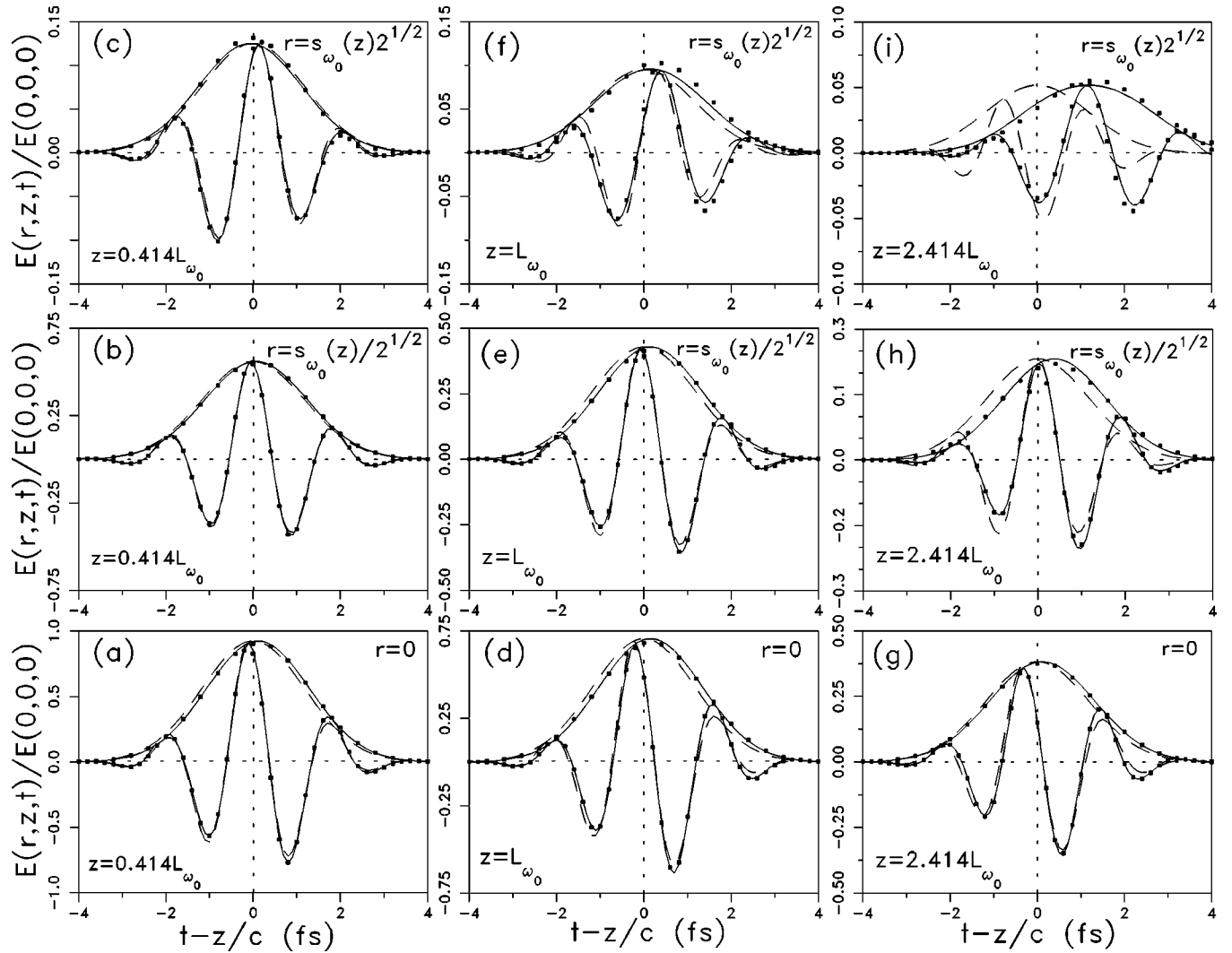


FIG. 6. Field amplitude and envelope for the pulsed Gaussian disturbance $E(r,0,t) = \exp(-r^2/s^2)\exp(-t^2/b^2)\exp(-i\omega_0 t)$ with $\omega_0 = 3.2 \text{ fs}^{-1}$, $b = 1.668 \text{ fs}$, and $s = 2 \text{ }\mu\text{m}$ at the points of space indicated in each figure. Dots: exact field. Solid curves: approximate second-order field of Eq. (40). Dashed curves: zeroth-order field.

We have also verified that the carrier phase at the caustic surface $r = s_{\omega_0}(z)/\sqrt{2}$ (central row) are nearly equal, as expected from Eq. (35), to the Gouy phase shift at the distance z . In fact, the carrier phases obtained from the numerical solution are (b) $\phi = -25^\circ$, (e) -46° , and (h) -68° , whereas the Gouy phase shifts at the same axial distances are -22.5° , -45° , and -67.5° . We note that the zero-order solution yields the rather wrong values -10° , -16° , and 2° .

In the above example, we have deliberately chosen a single-cycle pulse to test our analytical description of pulsed beams in the most difficult case ($\Delta\omega/\omega_0$ is as large as 0.44). The characteristics of the single-cycle pulsed Gaussian beam are accurately reproduced at points of space where the intensity is significant; specifically, up to radial distances where the intensity (amplitude) has decreased down to $\sim 1\%$ ($\sim 10\%$) of the on-axis intensity (amplitude). At larger radial distances, analytical and numerical values start to disagree significantly. The second derivatives of the amplitude and the

phase should then be included. Additional numerical simulations with longer pulses ($1\frac{1}{2}$ cycle, 2 cycle, ...) show that the region of validity of the first-order description extends up to much larger radial distances, where more significant pulse transformations take place.

Finally, Eq. (22) allows us to write an expression for the propagating field of pulsed Gaussian beams that carry the pulse transformations as given by our approximate analytical expressions. Equation (22) with $\varphi''_{\omega_0}(\mathbf{r}) = 0$ and $A_{\text{GVD}}(0, \tau) = A(0, \tau)$ simplifies to

$$\begin{aligned}
 E(\mathbf{r}, t) \simeq & \{ a_{\omega_0}(\mathbf{r}) A[0, t - \varphi'_{\omega_0}(\mathbf{r})] \\
 & + i a'_{\omega_0}(\mathbf{r}) (\partial/\partial t) A[0, t - \varphi'_{\omega_0}(\mathbf{r})] \} \\
 & \times \exp\{-i[\omega_0 t - \varphi_{\omega_0}(\mathbf{r}) - \phi]\}, \quad (40)
 \end{aligned}$$

where $a_{\omega_0}(\mathbf{r})$ and $\varphi_{\omega_0}(\mathbf{r})$ are the amplitude and phase of the Gaussian beam at the carrier frequency [Eqs. (26) and (27)], and $a'_{\omega_0}(\mathbf{r})$ and $\varphi'_{\omega_0}(\mathbf{r})$ are their first derivatives [Eqs. (36)

and (30)]. In Fig. 6 we compare the approximate expression (40) (solid curves) with the exact field (small squares) in the case of a single-cycle Gaussian pulse $A(0, \tau) = \exp(-\tau^2/b^2)$. By construction, the approximate expression fits to the exact field in the same region where the pulse transformations are accurately reproduced, i.e., inside the caustic surface of $\sim 1/100$ transversal decay of intensity.

B. Pulsed Bessel beam

As a second example, we study the field radiated by the pulsed Bessel disturbance

$$E(\mathbf{r}_\perp, t) = P(t)J_0(Kr) \quad (41)$$

of spectrum $\hat{E}_\omega(\mathbf{r}_\perp) = \hat{p}_\omega J_0(Kr)$, where $P(t) = A(0, t) \times \exp[-i(\omega_0 t - \phi)]$, $J_0(\cdot)$ is the Bessel function of zero order and first kind, and $K < \omega_0/c$ is a constant independent of frequency that determines the size of the transversal Bessel function. The above spectrally pure disturbance must be distinguished from the Bessel-x disturbance $\hat{E}_\omega(\mathbf{r}_\perp) = \hat{p}_\omega J_0(Kr)$, with $K \propto \omega/c$. Contrary to Bessel-x pulses, pulsed Bessel beams experience diffraction changes, which have been studied in Ref. [22] on the basis of numerical simulations. It has been shown that the pulse $P(t)$ broadens during propagation, while the transversal profile remains a $J_0(Kr)$ function [22]. This behavior can be easily understood from the diffraction-induced spectrum chirp.

The propagated spectrum is the well-known monochromatic Bessel beam

$$\hat{U}_\omega(\mathbf{r}) = J_0(Kr) \exp[i\sqrt{(\omega/c)^2 - K^2}z], \quad (42)$$

whose amplitude and phase are

$$a_\omega(\mathbf{r}) = |J_0(Kr)|, \quad (43)$$

$$\varphi_\omega(\mathbf{r}) = \sqrt{(\omega/c)^2 - K^2}z + \pi\theta[-J_0(Kr)], \quad (44)$$

where $\theta(\cdot)$ is the Heaviside step function. The last term in Eq. (44) adds a phase π at points where the Bessel function is negative. All derivatives of the amplitude with respect to frequency vanish, and the derivatives of the phase at the carrier frequency are

$$\varphi'_{\omega_0}(z) = \frac{z}{c} \frac{1}{\sqrt{1 - (Kc/\omega_0)^2}}, \quad (45)$$

$$\varphi''_{\omega_0}(z) = -\frac{K^2 c}{\omega_0^3} \frac{z}{[1 - (Kc/\omega_0)^2]^{3/2}}. \quad (46)$$

As indicated, they only depend on the coordinate z .

The characteristics of the propagating pulsed Bessel beam are then the following. The phase fronts

$$\omega_0 t - \sqrt{(\omega_0/c)^2 - K^2}z - \pi\theta[-J_0(Kr)] = \text{const.} \quad (47)$$

advance, according to Eq. (16), at the constant superluminal phase velocity

$$v^{(p)} = \frac{c}{\sqrt{1 - (Kc/\omega_0)^2}}. \quad (48)$$

The phase front

$$t = \frac{z}{c} \frac{1}{\sqrt{1 - (Kc/\omega_0)^2}} \quad (49)$$

is plane and propagates at the constant subluminal group velocity

$$v^{(g)} = c\sqrt{1 - (Kc/\omega_0)^2}. \quad (50)$$

As $a_\omega(\mathbf{r})$ does not depend on frequency, there are no amplitude spectral changes and, in particular, no redshift or blueshift of the carrier oscillations during propagation. Diffraction-induced spectrum chirp, given by Eq. (46), is always negative with absolute value growing linearly with propagation distance z , as in the propagation of a plane pulse in a medium with anomalous group velocity dispersion (negative second derivative of the propagation constant) $k''_{\omega_0} \equiv \varphi''_{\omega_0}(z)/z = -(K^2 c/\omega_0^3)[1 - (Kc/\omega_0)^2]^{-3/2}$. Accordingly, pulse broadening is constant at transversal planes $z = \text{const}$, and becomes sizeable at axial distances z of the order of the ‘‘dispersion length’’ $L_{\text{disp}} = 2(\Delta t_{\text{rms}})^2/|k''_{\omega_0}|$, where Δt_{rms} is the rms width of the initial pulse. From standard formulas for dispersive pulse propagation [11], the pulse duration propagation at any propagation distance is given by

$$\Delta t_{\text{rms}}(z) = \Delta t_{\text{rms}} \sqrt{1 + \frac{z^2}{L_{\text{disp}}^2}}. \quad (51)$$

All previous features are contained in the expression

$$E(\mathbf{r}, t) = A_{\text{GVD}}[\varphi''_{\omega_0}(z), t - \varphi'_{\omega_0}(z)] \times \exp[-i(\omega_0 t - \sqrt{(\omega_0/c)^2 - K^2}z - \phi)]J_0(Kr) \quad (52)$$

for the propagated field of pulsed Bessel beams, obtained from Eqs. (22) and (8). Equation (52) represents a pulse whose carrier oscillations propagate at the phase velocity $v^{(p)} > c$, and whose envelope propagates at $v^{(g)} < c$ along the z direction at the same time that broadens due to diffraction-induced GVD and is transversally modulated by the same function $J_0(Kr)$ at any propagation distance. In the particular case of a Gaussian initial envelope $A(0, \tau) = \exp(-\tau^2/b^2)$, Eq. (23) for A_{GVD} can be analytically carried out, as is well known, yielding

$$A_{\text{GVD}}[\varphi''_{\omega_0}(z), t - \varphi'_{\omega_0}(z)] = \frac{b}{b(z)} \exp\left\{-\frac{[t - \varphi'_{\omega_0}(z)]^2}{b^2(z)}\right\}, \quad (53)$$

with $b^2(z) = b^2 - 2i\varphi''_{\omega_0}(z)$. Then the propagated pulsed Bessel beam with Gaussian pulse envelope is given by

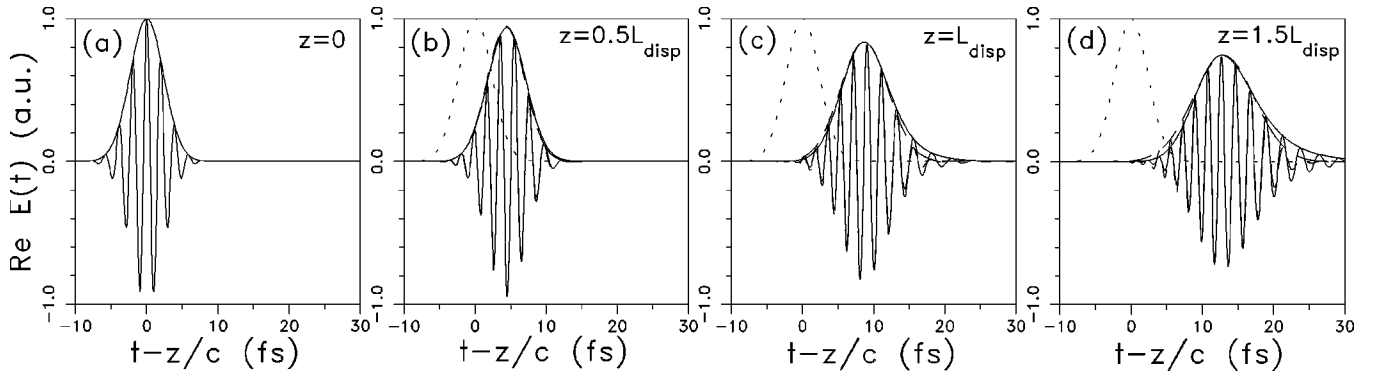


FIG. 7. Field amplitude and envelope for the pulsed Bessel disturbance $E(r,0,t)=J_0(Kr)\exp(-t^2/b^2)\exp(-i\omega_0 t)$ with $\omega_0=3.2 \text{ fs}^{-1}$, $b=3.34 \text{ fs}$, and $K=2.13 \times 10^3 \text{ mm}^{-1}$ at different positions of space. In all figures $r=0$ and z increases from (a) to (d). The dispersion length due to diffraction is $L_{\text{disp}}=2(\Delta t_{\text{rms}})^2/|k''_{\omega_0}|=0.126 \text{ mm}$ with $k''_{\omega_0}=\varphi''_{\omega_0}/z=-44.3 \text{ fs}^2/\text{mm}$. Solid curves: exact field. Dashed curves: approximate field of Eq. (54).

$$E(r,t)=\frac{b}{b(z)}\exp\left\{-\frac{[t-\varphi'_{\omega_0}(z)]^2}{b^2(z)}\right\}\times\exp[-i(\omega_0 t-\sqrt{(\omega_0/c)^2-K^2}z-\phi)]J_0(Kr). \quad (54)$$

In Fig. 7 we see the diffraction changes in temporal form of a pulsed Bessel beam with Gaussian envelope of parameters $\omega_0=3.2 \text{ fs}^{-1}$, $K=0.2\omega_0/c=2.13 \times 10^3 \text{ mm}^{-1}$ (transversal size of the Bessel function $2/K \approx 2\lambda_{\omega_0}$), $b=3.34 \text{ fs}$ (2 cycle), and $\phi=0$. The solid curves represent the exact pulse form $\text{Re } E(r,z,t)$ and $|A(r,z,t)|$ at several distances along the beam axis, numerically calculated from Eqs. (42) and (6) [out of axis the pulse form only changes by a factor $J_0(Kr)$]. The dashed curves represent the approximate field of Eq. (54), and the dotted curves represent the initial pulse propagating without change at speed c , for reference. The exact and approximate fields are almost indistinguishable; in particular, they peak at the same times [corresponding to a pulse traveling at the group velocity of Eq. (50), $v^{(g)}=2.94 \times 10^{-4} \text{ mm/fs}$ smaller than c] and they also have similar durations and peak amplitudes. The discrepancy in the trailing and leading parts of the pulse at distances of the order or larger than the dispersion length $L_{\text{disp}}=0.126 \text{ mm}$ are due to diffraction-induced third-order dispersion, which turns the envelope into an asymmetric function. As predicted, no significant redshift or blueshift is found.

IV. CONCLUSIONS

We have applied basic concepts of the propagation of three-dimensional wave packets to the description of diffraction (finite transversal size) effects on the propagation of ultrashort, few-optical-cycle pulses. Diffraction-induced pulse transformations in vacuum can be described in the same way as one-dimensional pulse transformations in a dispersive system. Previously described effects as pulse time delay (pulse front curvature), frequency blueshift and redshift of the optical oscillations, and pulse broadening, appear here classified as first-order and second-order diffraction-induced dispersion effects, which can be accurately quantified by simple analytical expressions. By analogy with dispersive pulse propagation, higher-order effects due to third-order dispersion and second-order gain dispersion can be easily introduced.

The application of this method to pulsed Gaussian beams allowed us to describe unknown characteristics such as the form of the pulse front surface within Rayleigh distance and superluminal group velocity outside. Approximate analytical expressions for the diffracted pulse can be written in terms of the well-known problem of pulse propagation with group velocity dispersion. Although we have restricted our attention to transformations of the pulse temporal form due to finite transversal size of the source, the same method can be used to characterize the effects of ultrashort pulse duration on transversal diffraction pattern. The results of this paper can be of use for the design of optical experiments with few-cycle optical pulses.

-
- [1] I. P. Christov, *Opt. Commun.* **53**, 364 (1985).
 - [2] C. J. R. Sheppard and X. Gan, *Opt. Commun.* **133**, 1 (1997).
 - [3] A. E. Kaplan, *J. Opt. Soc. Am. B* **15**, 951 (1998).
 - [4] G. P. Agrawal, *Opt. Commun.* **157**, 52 (1998).
 - [5] M. A. Porras, *Phys. Rev. E* **58**, 1086 (1998).
 - [6] C. F. R. Caron and R. M. Potvliege, *J. Mod. Opt.* **46**, 1881 (1999).
 - [7] M. A. Porras, *Opt. Lett.* **26**, 44 (2001).
 - [8] T. Brabec and F. Krausz, *Rev. Mod. Phys.* **72**, 545 (2000).
 - [9] M. Mehendale, S. A. Mitchell, J. P. Likforman, D. M. Villeneuve, and P. B. Corkum, *Opt. Lett.* **25**, 1672 (2000).
 - [10] E. Born and E. Wolf, *Principles of Optics* (Pergamon, Oxford, 1975).
 - [11] See, for example, G. P. Agrawal, *Nonlinear Fiber Optics* (Academic, New York, 1995).
 - [12] O. Svelto, *Principles of Lasers* (Plenum, New York, 1982).
 - [13] K. E. Oughstun and G. C. Sherman, *Electromagnetic Pulse Propagation in Causal Dielectrics* (Springer, Berlin, 1997).

- [14] J. Jones, *Am. J. Phys.* **42**, 43 (1974).
- [15] T. Brabec and F. Krausz, *Phys. Rev. Lett.* **78**, 3282 (1997).
- [16] M. A. Porras, F. Salazar-Bloise, and L. Vazquez, *Phys. Rev. Lett.* **85**, 2104 (2000).
- [17] M. A. Porras, *Opt. Lett.* **26**, 1364 (2001).
- [18] L. Ronchi and M. A. Porras, *Opt. Commun.* **103**, 44 (1993).
- [19] J. Lu and J. F. Greenleaf, *IEEE Trans. Ultrason. Ferroelectr. Freq. Control* **39**, 441 (1992).
- [20] D. Mugnai, A. Ranfagni, and R. Ruggeri, *Phys. Rev. Lett.* **84**, 4830 (2000).
- [21] M. A. Porras, R. Borghi, and M. Santarsiero, *Phys. Rev. E* **62**, 5729 (2000).
- [22] Z. Liu and D. Fan, *J. Mod. Opt.* **45**, 17 (1998).